

Multibanded Reduced Order Quadrature Techniques for Gravitational Wave Inference

Murdoc Newell¹, Alexis Boudon², and Hong Qi^{1,★}

¹ School of Mathematical Sciences, Queen Mary University of London, 327 Mile End Road, London, E14NS, United Kingdom

² Univ Lyon, Univ Claude Bernard Lyon 1, CNRS/IN2P3, IP2I Lyon, UMR 5822, F-69622, Villeurbanne, France

Received December 30, 2025

ABSTRACT

Reduced-order quadrature (ROQ) is commonly used to speed up parameter estimation in gravitational wave astronomy; however, the construction of ROQ bases can be computationally costly, particularly for longer duration signals. We propose a modified construction strategy based on PyROQ that accelerates this process by performing the basis search using multiband waveforms, without compromising the desired likelihood speed and accuracy. We use this altered method to construct a set of ROQs in the sub-solar mass range using the IMRPhenomXAS_NRTidalV3 waveform. We find a 20% to 30% decrease in basis size and a ~ 10 times decrease in basis construction time. We verify the altered method preserves the likelihood accuracy and maintains consistent parameter estimation results.

Key words. gravitational waves – reduced order quadratures – multiband

1. Introduction

The direct detection of gravitational waves has opened a new window into the universe, enabling the study of compact binary coalescences and other extreme astrophysical phenomena. Since the first detection of a binary black hole merger in 2015 (Abbott et al. 2016), the LIGO-Virgo-KAGRA detector network has observed hundreds of gravitational wave events, with compact binary mergers being the dominant source class (Abbott et al. 2021, 2023; Abac et al. 2025). Each detection requires sophisticated parameter estimation techniques to infer the physical properties of the source systems.

Bayesian parameter estimation for gravitational wave signals involves evaluating the likelihood function millions of times across the multi-dimensional parameter space. For each likelihood evaluation, the overlap integral between the observed detector data and theoretical waveform templates must be computed across the full frequency band of the detectors, typically from tens to thousands of Hertz. The computational cost scales linearly with both the number of frequency samples and the complexity of the waveform model. For longer-duration signals, such as those from sub-solar mass (SSM) compact objects which remain in the detector sensitivity band for extended periods, this computational burden becomes prohibitive, with individual parameter estimation analyses requiring weeks or even months of computing time.

Reduced-order quadrature (ROQ) methods have emerged as a powerful solution to this computational challenge (Canizares et al. 2015; Smith et al. 2016a; Qi & Raymond 2021; Morisaki et al. 2023). By constructing reduced bases that accurately represent the space of possible waveforms, ROQ techniques enable the overlap integrals to be evaluated using only a small subset of frequency points, achieving speedups of two

to three orders of magnitude while maintaining likelihood accuracy to within acceptable tolerances. Our previous code PyROQ implements an efficient algorithm for constructing these reduced bases.

However, the construction of ROQ bases itself presents a computational bottleneck. The search algorithm requires generating large training sets of waveforms, often millions of templates, and performing numerous inner product evaluations at each iteration. For long-duration signals like subwith hundreds of thousands of frequency samples, this construction process can take days to weeks on high-performance computing clusters, limiting the ability to generate ROQ bases for emerging waveform models or extended parameter ranges.

In this work, we present a modified ROQ construction strategy that leverages multi-banding techniques (Vinciguerra et al. 2017) to accelerate the basis construction without compromising the accuracy of the final likelihood evaluations. Multi-banding exploits the fact that gravitational wave signals from compact binary inspirals are not uniformly sampled in time across all frequencies, as lower frequencies contain proportionally more signal cycles than higher frequencies. By using frequency-dependent resolution during the basis search, with finer spacing at low frequencies and coarser spacing at high frequencies, we reduce the number of frequency samples by nearly an order of magnitude while preserving the essential features needed to construct accurate reduced bases.

We apply this multibanded construction method to generate ROQ bases for the IMRPhenomXAS_NRTidalV3 waveform model in the SSM regime, a parameter space of particular interest for searches targeting primordial black hole binaries and other exotic compact objects. Our results demonstrate that the multibanded approach reduces basis construction time by a factor of 5 to 20 times while simultaneously decreasing the basis size by 20-30%. We validate these bases through comprehensive

* Corresponding author: hong.qi@ligo.org

likelihood comparisons and full parameter estimation injection studies, confirming that the multibanded construction introduces no detectable biases or accuracy degradation in recovered source parameters.

The structure of this paper is as follows. In Section 2, we review the fundamentals of gravitational wave parameter estimation, the ROQ formalism, multi-banding techniques, and our implementation strategy. Section 3 presents our construction results, likelihood validation tests, and parameter estimation comparisons. We conclude in Section 4 with a discussion of the implications for future gravitational wave analyses and potential extensions of this methodology.

2. Methodology

2.1. Gravitational Wave Inference

Gravitational wave inference is performed to find the probability density function for a set of source parameters θ used to model a gravitational wave signal depending on the detectors' observed strain data, d . This PDF or *posterior* can be defined using Bayes Theorem:

$$p(\theta|d) \propto \mathcal{L}(d|\theta)\pi(\theta), \quad (1)$$

where $\mathcal{L}(d|\theta)$ is the *likelihood* function of the data given the source parameters and $\pi(\theta)$ is the *prior* probability for the source parameters. The highest computational cost is in evaluating the likelihood.

The detector strain can be modeled as a combination of a gravitational wave signal, $h(\theta)$, and noise, n , such that $d = h(\theta) + n$ (Finn 1992). Thus, we define the log-likelihood function as

$$\begin{aligned} \log \mathcal{L}(d|\theta) &= -\frac{1}{2}(d - h(\theta), d - h(\theta)) \\ &= -\frac{1}{2}(d, d) + (d, h(\theta)) - \frac{1}{2}(h(\theta), h(\theta)). \end{aligned} \quad (2)$$

The overlap integral (\cdot, \cdot) is defined as

$$(d, h(\theta)) = 4\Re \Delta f \sum_{k=1}^L \frac{\tilde{d}^*(f_k) \tilde{h}(f_k; \theta)}{S_n(f_k)}, \quad (3)$$

where $S_n(f_k)$ is the power spectral density (PSD) of the detectors' noise. We can approximate the number of sampling points L over an observation time $\tau = 1/\Delta f$ as $L \approx \text{int}([f_{\text{high}} - f_{\text{low}}]\tau)$, where f_{low} to f_{high} is the detector frequency range. Longer duration signals increase the number of terms in Eq. 3, and more complex waveforms with a greater number of parameters θ need more extensive sampling; more evaluations of Eq. 3 are required. The computational costs of this impose a bottleneck on gravitational wave inference.

2.2. Reduced Order Quadratures

In this section, a brief overview of the ROQ rule, along with its construction, is given. More detailed explanations can be found in (Smith et al. (2016b)). A gravitational waveform, $h(f_i; \theta)$, and its modulo squared, $|h(f_i; \theta)|^2$, can be represented by empirical interpolants, given by

$$h(f_i; \theta) \approx \sum_{j=1}^{N_L} B_j(f_i) h(F_j; \theta), \quad (4a)$$

$$|h(f_i; \theta)|^2 \approx \sum_{k=1}^{N_Q} C_k(f_i) |h(\mathcal{F}_k; \theta)|^2, \quad (4b)$$

where $B_j(f_i)$, $C_k(f_i)$ are the reduced (RBs), and $\{F_j\}_{j=1}^{N_L}$, $\{\mathcal{F}_k\}_{k=1}^{N_Q}$ are the interpolant nodes. By substituting Eq. 4a and 4b into the log likelihood, Equation 2, the likelihood can approximated as

$$\log \mathcal{L} \approx -\frac{1}{2}(d, d) + (d, h(\theta))_{\text{ROQ}} - \frac{1}{2}(h(\theta), h(\theta))_{\text{ROQ}}, \quad (5)$$

where the overlaps are calculated using precomputed quadrature weights.

Once found, the number of terms required to solve the ROQ likelihood is $N_L + N_Q$, leading to an $L/(N_L + N_Q)$ speedup. The aim during ROQ construction is to minimize $N_L + N_Q$ whilst maintaining a desired threshold accuracy.

A brief overview of how the ROQs basis elements are found using the PyROQ code will be provided, with more detailed explanations available in (Qi & Raymond 2021). The process begins with the generation of a large training set of waveform parameters θ . After an initial basis element is found, an iterative process occurs where the parameters associated with the waveform with the highest maximum empirical interpolation error are added to the basis. This process terminates once the entire training set falls below a threshold empirical interpolation error. The dominant computational cost occurs at this stage, as it requires a high volume of generated waveforms and inner product evaluations. This means that for longer or more complex waveforms, computational cost can be high.

2.3. Multibanding

In traditional PE methods, for a signal of duration τ , the frequency resolution is fixed at $\Delta f = \tau^{-1}$, with the total number of samples given by $N = (f_{\text{max}} - f_{\text{min}})\tau$. The amount of time, t , an inspiral signal spends at frequency, f , is given by (Cutler & Flanagan 1994)

$$t(f) = 5(8\pi f)^{-8/3} \mathcal{M}^{-5/3}, \quad (6)$$

where \mathcal{M} is the chirp mass of the source object. Therefore, using a uniform frequency grid will end up with certain parts of the signal being oversampled. multibanding takes advantage of this by having the frequency resolution be dependent on the frequency itself. More specifically, the full frequency range is split into multiple bands, each of which has different but uniform frequency resolutions. A visual representation of this can be found in Figure 1. For this work, we construct multibands using the following structure, built on the base frequency spacing $\Delta f_0 = 1/\tau$,

$$\Delta f(f) = \begin{cases} \Delta f_0, & f_{\text{min}} \leq f < f_1 \\ 2\Delta f_0, & f_1 \leq f < f_2 \\ \vdots & \vdots \\ 2^N \Delta f_0, & f_N \leq f \leq f_{\text{max}}. \end{cases} \quad (7)$$

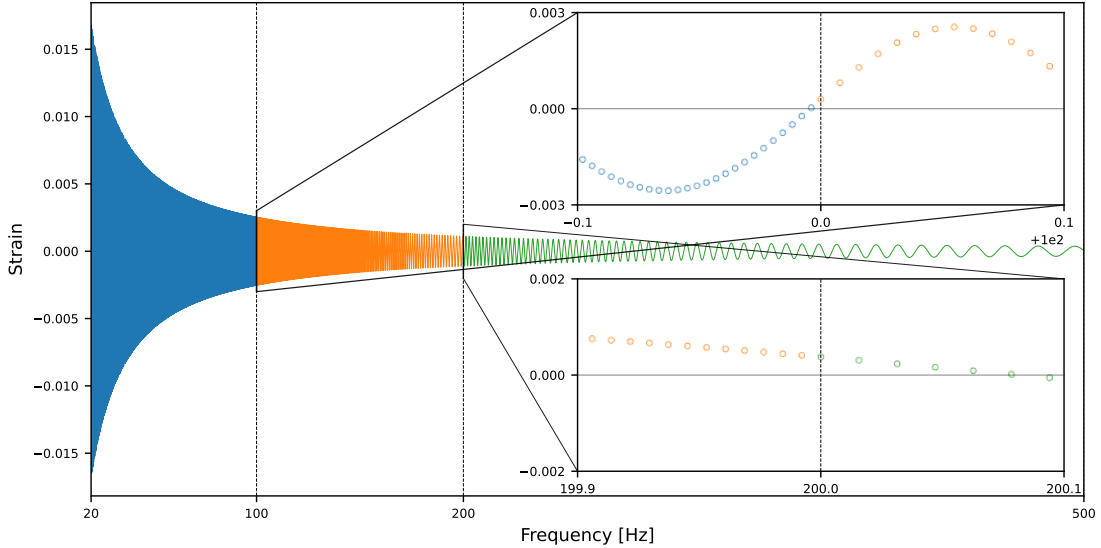


Fig. 1: Illustration of a multibanded waveform in the frequency domain. The larger panel shows the full waveform, with the band boundaries marked using dashed vertical lines at $f = 100\text{Hz}$, and 200Hz . The multiple colors represent the different Δf used across each band. The upper and lower smaller panels show a zoomed-in view of the same waveform at the $f = 100\text{Hz}$ and $f = 200\text{Hz}$ band boundaries, respectively, highlighting the change in Δf across bands.

Table 1: Comparison in ROQ construction using the standard and multibanded construction method.

Bases	multibanding	# Frequency Samples	Basis size		Construction Time [hour]	
			Linear	Quadratic	Linear	Quadratic
256s	No	916481	303	98	105.78	37.35
256s	Yes	110081	233	68	7.99	5.85

2.4. Implementing multiBanding in ROQ Construction

For this work, we apply multibanding only during ROQ basis greedy search and does not affect the final likelihood evaluation.

1. The first stage involves generating the multibanded frequency array. A key detail is that the same chosen multibanded array must be used for all waveforms across the whole parameter range, for which the ROQs will be built.
2. The next step is to generate the training dataset as usual. Each data point consists of a set of parameter values, θ_i , which represent a waveform found within the desired parameter range.
3. The PyROQ reduced basis search algorithm, as found in Qi & Raymond (2021), is performed. The difference is that the training waveforms are evaluated using the multibanded frequency array. The parameter values of the RB elements, θ_i^{MB} , are stored.
4. Using the multibanded parameter values θ_i^{MB} , the RB is reconstructed using the full frequency array, and standard ROQ construction continues.

3. Results

3.1. ROQ and Multibanded ROQ Construction Comparison

In this section, we compare the performances of our multibanded construction method with the standard construction method found in PyROQ. We then show how our method provides both ROQ construction speed-up and basis size reduction with negligible loss in accuracy.

For this, we use the `IMRPhenomXAS_NRTidalv3` waveform model (Abac et al. 2024), as implemented in the LIGO Algorithm Library (LAL) (LIGO Scientific Collaboration et al. 2018). This phenomenological model approximates inspiral-merger-ringdown signals for aligned spin systems. It is also capable of incorporating tidal effects, such as those found in BNS and NSBH systems. This waveform was chosen as it produces accurate long-duration signals in sub-solar mass ranges, which is an area that is proving computationally intensive for current ROQ construction methods.

PyROQ was used to construct both bases, with identical parameter ranges used in both. For the 256s signal, the chirp mass range was $0.995 M_{\odot}$ to $1.005 M_{\odot}$, with mass ratios ranging from 1 to 4.1. The dimensionless spin magnitude, $a_{1,2}$, ranging from 0 to 1, and the tidal deformabilities, $\lambda_{1,2}$, ranging from 0 to 5000. The frequency range is 20 Hz to 3600 Hz. The dataset for the standard ROQ used a uniform frequency step size of $\Delta f_0 = 1/256 \text{ Hz}$, whereas for the multibanded method, the step size used is given by

$$\Delta f(f) = \begin{cases} \Delta f_0, & 20 \text{ Hz} \leq f < 100 \text{ Hz} \\ 2 \Delta f_0, & 100 \text{ Hz} \leq f < 200 \text{ Hz} \\ 4 \Delta f_0, & 200 \text{ Hz} \leq f < 500 \text{ Hz} \\ 8 \Delta f_0, & 500 \text{ Hz} \leq f < 1000 \text{ Hz} \\ 16 \Delta f_0, & 1000 \text{ Hz} \leq f \leq 3600 \text{ Hz}. \end{cases} \quad (8)$$

This means each multiband waveform used during construction has 110,081 frequency samples, compared to the 916,481 used in

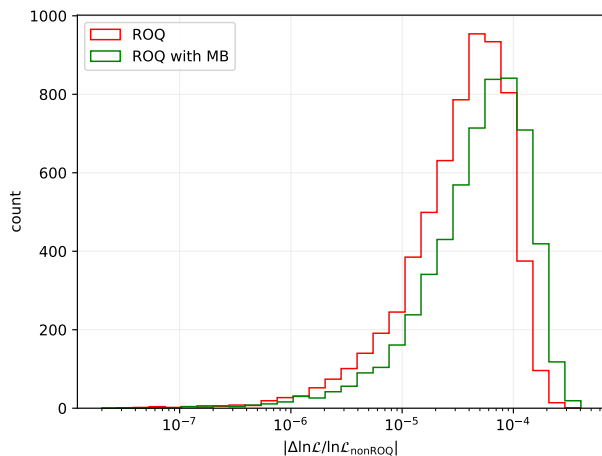


Fig. 2: The distributions of the likelihood errors between the full likelihood and the ROQ likelihood (red) and the multiband ROQ likelihood (green), respectively, for 6400 randomly drawn injected waveforms. The samples were drawn from the parameter space used to construct the 256s bases, as described in Section 2.3. All samples were found with likelihood errors less than 7×10^{-3} .

the standard method, a ~ 9 times decrease. The threshold tolerance is 10^{-5} and 10^{-10} for the linear and quadratic bases respectively. A training dataset of 1 million waveforms was used in both constructions. Both bases were constructed using 32 CPUs, with the linear bases using 256GB RAM and the quadratic bases using 64GB RAM on the LIGO data grid.

The results for the two constructions can be found in Table 1. Comparing the 256s bases, we see an approximate 30% decrease in the basis size (303 versus 233 for linear and 98 versus 68 for quadratic). The biggest change is found in the overall construction time with the linear basis constructed in 7.99 hours rather than 105.78 hours, a ~ 13 times speed up, and the quadratic constructed in 5.83 hours rather than 37.35 hours, a ~ 6 times speed up. More exact values are given in Table 2.

These results show that introducing multibanding during the ROQ basis search both speeds up the construction whilst decreasing the overall basis size. For long-duration signals, such as the 256s ones used here, this improvement is especially apparent with the construction time going from a few days to just several hours.

Basis Type	Basis size change	Construction speedup
Linear	-23.1%	13.2 \times
Quadratic	-30.6%	6.38 \times

Table 2: Table showing the basis size decrease and basis construction time speed up, going from the standard ROQ construction to the multibanded ROQ construction.

3.2. GW Likelihood Comparison

We now calculate the likelihood error of our multiband constructed `IMRPhenomXAS_NRTidalv3` ROQ relative to the full

likelihood and the basis built using the standard PyROQ method. This is done using `BILBY` (Ashton et al. 2019).

To do this, we generated 6400 samples from our parameter space defined in Section 3.2. The percentage error between the difference in likelihoods and the full likelihood is calculated. The distribution for the likelihood error between the multiband constructed ROQs and the full likelihood is shown in Figure 2. From this, we see that the likelihood errors do not exceed 7×10^{-3} . Comparing the likelihood error with the standard ROQ constructed bases, we do see a slight increase with the overall error. However, we will see later that this error increase proves negligible during a PE run.

3.3. Parameter Estimation

To validate the accuracy of our multiband constructed basis, we performed a set injection parameter estimation run. The signals were simulated based on the prior values given in Table 3.2, and injected into Gaussian noise, using A+ projected PSDs. The source parameters were recovered using both the standard PyROQ basis (in orange) and the basis constructed with the multiband construction method (in blue), with the posteriors from one of the runs shown in the corner plots of Figure 3.

The parameter estimation was performed with `BILBY`, using the `dynesty` sampler with `nlive=1000` and `nact=10`. Twenty injection runs were performed, with all jobs running on the LIGO data grid using 16 CPUs and 16GB of RAM each. We showcase one example injection signal, with chirp mass $1.0017M_{\odot}$, mass ratio 2.19, dimensionless spins $a_{1,2} = \{0.0465, 0.0518\}$, and tidal deformabilities $\Lambda_{1,2} = \{3566, 3683\}$. Both the injected values and the parameter estimation priors for the injected signal are given in Table 3. For the injection in Figure 3, the PE run time using the multiband constructed ROQs was 2.99 hours compared to 2.93 hours using the standard constructed ROQs, suggesting little change in PE run times using the new method.

The corner plot shows the results for the intrinsic source parameters, namely the chirp mass \mathcal{M} , mass ratio q , spin magnitudes $a_{1,2}$, and tidal deformabilities $\Lambda_{1,2}$. Looking at the figure, we see that both bases show clear agreement across all the parameters. No obvious biases are observed, and the credible intervals are consistent through both methods. This was consistent across all twenty runs, and shows that using the multiband constructed ROQs has no downstream impact on the parameter estimation.

4. Conclusions

We have described a change to the algorithm implemented in PyROQ, which significantly speeds up the construction of reduced bases for gravitational wave waveforms, by utilizing multibanded waveforms during the basis search.

We used our multiband ROQ construction method to construct a subsolar mass basis for the `IMRPhenomXAS_NRTidalv3` waveform model. Comparing this to a ROQ basis constructed using the standard PyROQ method over identical parameter ranges, we found a $\sim 30\%$ decrease in basis size, and a ~ 13 and ~ 9 times decrease in construction time for the linear and quadratic bases, respectively. We also demonstrated our basis in a PE run, and found that the altered method had no affect on the final PE results relative to the standard PyROQ constructed bases.

The constructed bases for `IMRPhenomXAS_NRTidalv3` are the first to be built in subsolar mass ranges, and demonstrate the

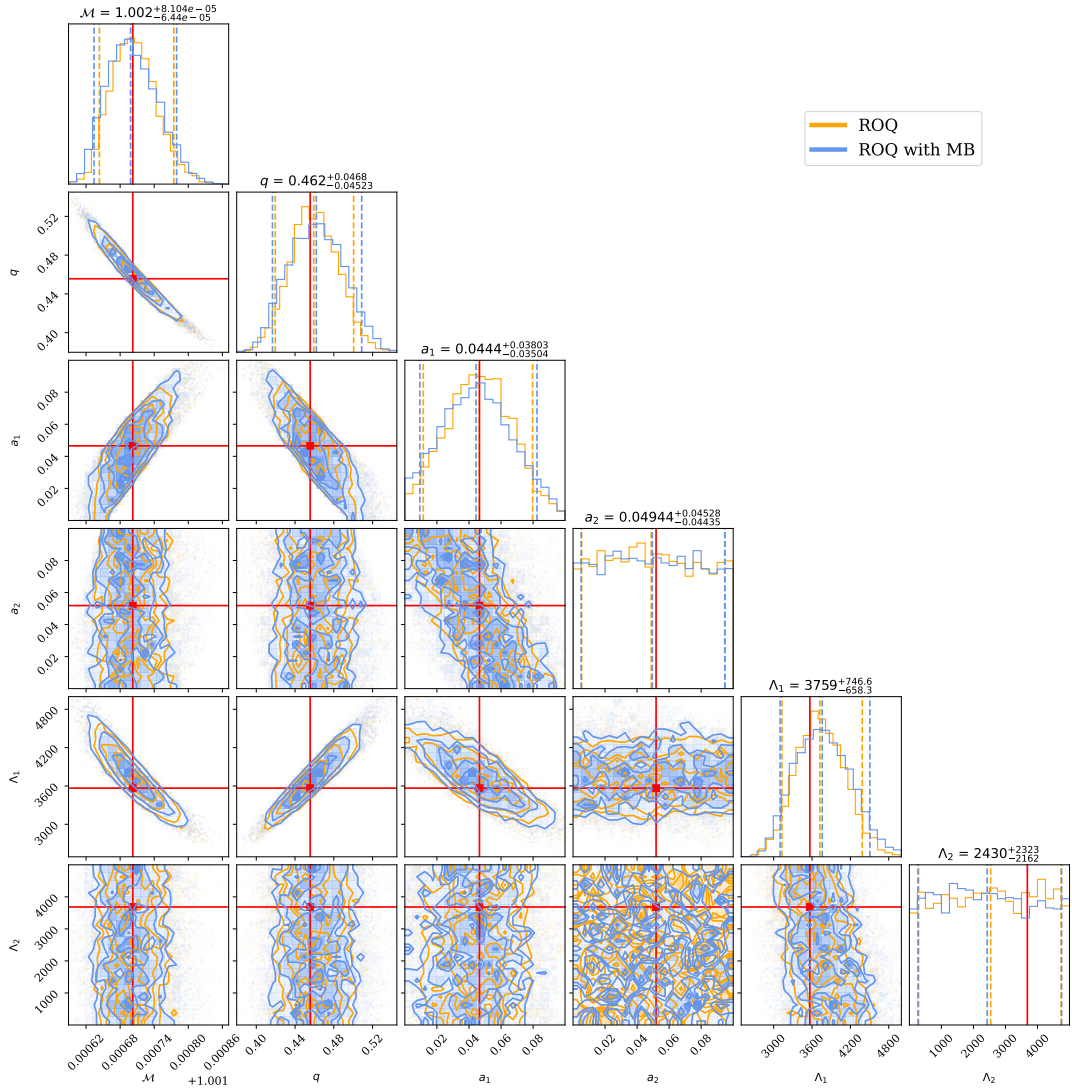


Fig. 3: Corner plots comparing the posterior distributions between the standard PyROQ method (blue) and the multibanded construction method (orange). The parameter values for the injected waveform is given by the red lines. The dashed lines show the median, and 1σ credible interval.

Table 3: The parameter values for the injected waveform shown in Figure 3, and the distribution and ranges used as the prior for the PE injection analysis.

Parameter (Symbol) [Unit]	Injection values	PE prior
Source-frame chirp mass (M_c) [M_\odot]	$1.0017 M_\odot$	Uniform [0.995, 1.005] M_\odot
Source-frame mass ratio (q)	2.19	Uniform [1, 4.1]
Dimensionless primary NS spin (a_1)	0.0465	Uniform [0, 0.05]
Dimensionless secondary NS spin (a_2)	0.0518	Uniform [0, 0.05]
Luminosity distance (d_L) [Mpc]	24.27 Mpc	Square power law [10, 50] Mpc
Right ascension (α) [radian]	0.945	Uniform [0, 2π]
Declination (δ) [radian]	1.97	Uniform Cosine
Inclination angle (θ_{JN}) [radian]	0.585	Uniform Sine [0, π]
Polarization (Ψ) [radian]	0.448	Uniform [0, π]
Tidal deformability of primary NS (Λ_1)	3566	Uniform [0, 5000]
Tidal deformability of secondary NS (Λ_2)	3683	Uniform [0, 5000]

capabilities of this new method. This will significantly reduce the computational cost for any parameter estimation of these longer-duration signals. Future work will focus on further implementing

this method, particularly in constructing ROQs for long-duration waveforms for the next-generation detectors.

280 *Acknowledgements.* We are grateful for the computational resources provided by LIGO Laboratory and the Leonard E Parker Center for Gravitation, Cosmology and Astrophysics at the University of Wisconsin-Milwaukee and supported by National Science Foundation Grants PHY-0757058, PHY-0823459, PHY-1626190, and PHY-1700765. We especially thank the computing resources provided by Digital Research Alliance of Canada through two consecutive grants, the DRAC RPP #1012 and the Compute Canada Allocation Award #696 to the University of British Columbia. We also thank the Hawk supercomputing system provided by Cardiff University. This material is based upon work supported by NSF's LIGO Laboratory which is a major facility fully funded by the National Science Foundation.

290 **References**

Abac, A., Dietrich, T., Buonanno, A., Steinhoff, J., & Ujevic, M. 2024, Phys. Rev. D, 109, 024062

Abac, A. G. et al. 2025 [[arXiv:2508.18082](https://arxiv.org/abs/2508.18082)]

Abbott, B. P., Abbott, R., Abbott, T. D., et al. 2016, Phys. Rev. Lett., 116, 061102

Abbott, R. et al. 2021, Phys. Rev. X, 11, 021053

Abbott, R. et al. 2023, Phys. Rev. X, 13, 041039

Ashton, G., Hübner, M., Lasky, P. D., et al. 2019, The Astrophysical Journal Supplement Series, 241, 27

Canizares, P., Field, S. E., Gair, J., et al. 2015, Phys. Rev. Lett., 114, 071104

Cutler, C. & Flanagan, E. E. 1994, Phys. Rev. D, 49, 2658

Finn, L. S. 1992, Phys. Rev. D, 46, 5236

LIGO Scientific Collaboration, Virgo Collaboration, & KAGRA Collaboration. 2018, LVK Algorithm Library - LALSuite. Free software (GPL)

Morisaki, S., Smith, R., Tsukada, L., et al. 2023, Phys. Rev. D, 108, 123040

Qi, H. & Raymond, V. 2021, Phys. Rev. D, 104, 063031

Smith, R., Field, S. E., Blackburn, K., et al. 2016a, Phys. Rev. D, 94, 044031

Smith, R., Field, S. E., Blackburn, K., et al. 2016b, Phys. Rev. D, 94, 044031

Vinciguerra, S., Veitch, J., & Mandel, I. 2017, Class. Quant. Grav., 34, 115006